Underestimation of strong wind speeds offshore in ERA5: evidence, discussion, and correction

Rémi Gandoin[1], Jorge Garza[1]

[1]C2Wind ApS, Fredericia, 7000, Denmark.

5   *Correspondence to*: R. Gandoin (rga@c2wind.com)

Abstract. Offshore Wind power plants have become an important element of the European electrical grid. Studies of metocean site conditions (wind, sea state, currents, water levels) form a key input to the design of these large infrastructure projects. Such studies heavily rely on reanalysis datasets which provide decades-long model time series over large areas. In this article, we address a known deficiency of one these reanalysis datasets, ERA5, namely that it underestimates strong wind speeds

10   offshore. For doing so, comparisons are made against CFSR/CFSv2 reanalyses as well as high quality wind energy specific in-situ measurements from floating LiDAR systems. The ERA5 surface drag formulation and its sea state dependency are analysed in detail, the conditions of the bias identified, and a correction method is suggested. The article concludes with proposing practical and simple ways to incorporate publicly available, high-quality wind energy measurement datasets in air-sea interaction studies alongside legacy measurements such as met buoys.

1 Introduction

Offshore wind power plants help reduce carbon emissions from the Power sector. They have gradually evolved from small demonstration projects (Vindeby, commissioned in 1991) to commercial-scale demonstration projects (Horns Reef 1, Nysted) in the early 2000s. Today, they stand as integral components of the European power grid (ENTSO-E, 2024).

Atmospheric Boundary Layer (ABL) wind datasets from Numerical Weather Prediction modelling systems (NWP models) are

20   routinely used for the purpose of assessing the offshore wind resource and for characterising sea state, water level and current conditions at offshore wind farm locations (NWP models provide inputs to hydrodynamic- and spectral wave models). Global reanalysis datasets such as CFSR (Saha et al., 2010), CFSv2 (Saha et al., 2014) and ERA5 (Hersbach et al., 2020) are widely used for these purposes as they are publicly available, free of charge, and cover long periods (decades).

Despite performing among the best (Ramon et al., 2019), the NWP model used for producing ERA5 suffers from a major

25   drawback for engineering purposes: it underestimates strong wind speeds offshore close to the surface, for instance at 10 m (a nominal elevation often used for hydrodynamic- and spectral wave modelling), see (Bentamy et al., 2021), (Alday et al 2021), (Solbreke et al., 2021), (Spangehl et al., 2023) and (Meyer et al., 2023). Therefore, for engineering applications the ERA5 10 m wind speed values are often corrected to ensure that site conditions design values are not underestimated, see for instance (DHI, 2023) (for design, slightly conservative values are typically desirable). As a result, and despite their shortcomings

30 (differences in land/sea masks and grid resolution, poorer correlation with in-situ measurements, no wind speed time series close to a modern turbine hub height), CFSR and CFSv2 remain, in the authors' experience, the preferred datasets for driving engineering hydrodynamic- and spectral wave modelling systems.

This ERA5 bias has not been widely discussed in the scientific literature, and it may not be clear to all ERA5 users that the data need to be corrected. Also, the methods published so far only partially address the bias: most often, they correct 10 m

35 winds only, and/or use site-specific corrections. The present article proposes a novel approach to both topics. After having provided elements of wind speed modelling in Sect. 1, we compare ERA5 and CFSv2 model time series at selected locations, with each other and against in-situ measurements in Europe and America in Sect. 2. The ERA5 strong wind bias is discussed in Sect. 3: a detailed analysis of the ERA5 drag formulation is provided and a simple correction method is suggested for wind speeds between 10 and 100 m using analytical ABL wind profile expressions from the literature. The measurement datasets

40 all come from high-quality, publicly available met mast and Floating LiDAR System (FLS) datasets; these are described in Sect. 1.

The main objectives of this article are 1) presenting evidence of the ERA5 underestimation of strong wind speeds, 2) discuss the reason for this underestimation, and propose a simple corrective method and 3) argue for using publicly available, high quality FLS measurements and met mast datasets for air-sea interaction studies, along with legacy measurements such as met

45 buoys. In Sect. 4, and with references to the recent literature, suggestions are made regarding practical actions and research initiative.

This article provides references to recent works regarding air-sea interaction and drag formulations. Yet, it does not take a scientific stand on the nature of these interactions. Instead, it merely tries to bring a practitioner's perspective to this long-lasting discussion, that is: for design purposes, an accurate depiction of both wind *and* sea state in reanalysis datasets is

50 required, and useful, quality datasets are readily available for validation work.

1.1 Elements of wind profile modelling

As explained for instance in (Peña et al., 2008) and its references such as (Stull, 1988), in the layer close to the surface where the Monin-Obukhov Similarity Theory (MOST) is valid, the mean wind speed U at a given elevation z above the surface is given by:

$$U(z) = \frac{u_{*0}}{\kappa}\left(\ln\left(\frac{z}{z_0}\right) + \psi_m\left(\frac{z}{L}\right)\right) \tag{1}$$

55

where u_{*0} is the friction velocity at the surface, z_0 is the roughness length, κ is the Von Karman constant (here taken equal to 0.4), L is the Obukhov length and ψ_m is an atmospheric stability-dependent function derived from experiments. Above the surface layer, this expression needs to be supplemented with additional terms: the height of the boundary layer z_i and a length scale L_{MBL} which is a characteristic length scale of the eddies in the ABL, see originally (Gryning et al, 2007) and its references.

60

Over water, the Charnock relationship is used for linking roughness length and friction velocity, see (Peña et al., 2008) and Eq. (3.26) of (ECMWF, 2016a):

$$z_0 = \alpha_{\mathrm{Ch}} \cdot \frac{u_{*0}^2}{g} + \alpha_{\mathrm{M}} \cdot \frac{\nu}{u_{*0}} \tag{2}$$

65   where α_{Ch} and α_{M} are sea state-dependent parameters and ν is the air kinematic viscosity (term only relevant for very small wind speeds). Formulations (1) and (2) are widely used in Numerical Weather Prediction (NWP) modelling systems such as the Global Forecast System (GSF), the Integrated Forecast System (IFS) or the Weather Research and Forecasting (WRF) Model. The term α_{Ch} is referred to as the Charnock parameter and is either kept constant (for instance in (Peña et al., 2008) or in CFSR/CFSv2, see (Renfrew et al., 2002)) or made dependent on sea state conditions. In this article, we focus on the IFS

70   Cy41r2 (ERA5) implementation, see Eq. (3.11) of (ECMWF, 2016b), where the atmospheric- and ocean models are coupled via:

$$\alpha_{\mathrm{Ch}} = \frac{\hat{\alpha}}{\sqrt{1 - \frac{\tau_{\mathrm{w}}}{\tau}}} \tag{3}$$

where τ is the wind stress (u_{*0}^2), τ_w is the wave stress (from the waves to the atmosphere) and $\hat{\alpha}$ is a constant. For all practical purposes, a drag neutral coefficient $C_{\mathrm{d,n}}$ can be derived, and often used for comparing model- and measurement results:

75

$$C_{\mathrm{d}}^2 = \frac{u_{*0}}{U_{\mathrm{n}}} = \frac{\kappa}{\ln\left(\frac{z}{z_0}\right)} \tag{4}$$

Where U_{n} is the wind speed evaluated using Eq. (1) and $\psi_m(z/\infty) = \psi_m(0) = 0$ (negligible buoyancy).

1.2 Measurement data description

In this article, we use well documented and validated, high-quality, publicly available wind energy measurement datasets such as Floating LiDAR Systems (FLS) and a met mast (cup anemometer); see Figure 1. Legacy instruments such a met buoys have

80   been left out intentionally due to the poor quality and traceability of these measurements in comparison with the former datasets. A discussion is provided in Sect. 4 on future works and the advantages of adding such wind energy measurements alongside legacy instruments to decrease modelling uncertainty.

The measurements have been chosen from the comprehensive list of datasets available on the Wind Resource Assessment Group wiki page[1], their locations are marked in red in Figure 2 and a high-level description is provided in Table 1 (except for M6 and 62001, where no measurement data are used). All measurement locations lie far offshore, where land/sea mask effects are negligible for the wind directional bins selected for the analyses (see Sect. 2.3).

2   Figure 1: Photographs of the Floating LiDAR Systems (left: Fugro, middle: Eolos) as well as the IJmuiden mast (right). Sources: Fugro, Eolos, Wind op Zee.

3   Table 1: High-level description of the measurement datasets used in this article. Detailed information can be found in the references provided in the table.

ID	Lon °E	Lat °N	Type	Period	Source	References
IJM	3.436	52.998	Mast (cups)	Nov11-Mar16	Wind op Zee	(Quaeghebeur and Zaaijer, 2020)
TNWA	5.551	54.018	FLS	Jun19-Jun20	RVO	(Fugro, 2022)
E05	-72.715	39.969	FLS	Aug19-Sep21	NYSERDA	(EOLOS, 2020)
E06	-73.429	39.546	FLS	Sep19-Mar22	NYSERDA	(EOLOS, 2020)
Lot 1	6.301	56.628	FLS	Nov21-Nov23	ENS	(Fugro, 2023)
Lot 2	6.457	56.344	FLS	Nov21-Nov23	ENS	(Fugro, 2023)

All FLS measurements have been validated as per the Carbon Trust Offshore Wind Accelerator Roadmap Stage 3 (Carbon Trust, 2018). That is: both types of LiDAR and FLS have been validated dozens of times against reference measurements (cups, or LiDAR validated against cups), and these tests have repeatedly shown mean relative deviations smaller than 2%. Examples of validations are provided in Fig. A1 and A2 in Appendix A. Large number of publicly available validation reports have been collected by the authors, see the supplementary material to this paper. For the specific case of the Fugro FLS, from the RVO campaigns[2] 16 validation reports are available together with additional studies such as (Kelberlau, 2022) and

---

[1] See https://groups.io/g/wrag/wiki/13236.

[2] See https://offshorewind.rvo.nl/

100   (Kelberlau and Mann, 2022) showing similarly very small deviations against several cup anemometer measurements offshore. For the EOLOS FLS, three validation reports are available in the above-mentioned online repository, and (Araújo da Silva, 2022) provides a thorough description and validation of the device at the IJmuiden met mast.
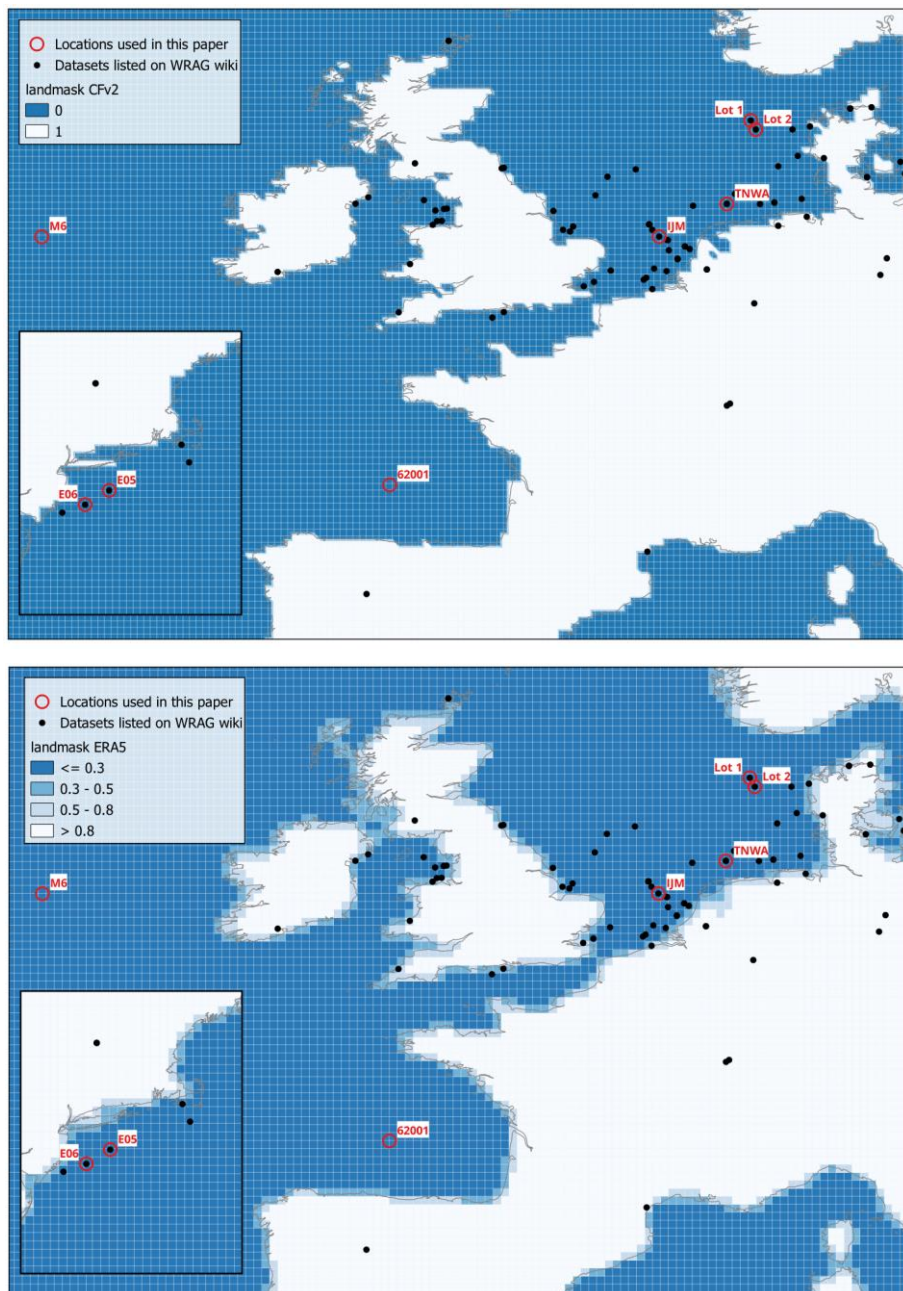
Figure 2:Location of the publicly available wind energy specific wind datasets (black dots), together with the analysis locations used for this paper. The two maps show land/sea masks for CFSv2 (top) and ERA5 (bottom).

105

All FLS used in this study are equipped with ZX Lidars continuous wave LiDARs; see (Knoop et al., 2021) for a research validation study. The 10-minute data have been filtered using a regular filter based on the average number of valid samples during one scan (so-called minimum number of packets); it is here set to 18. Fugro uses a threshold of 9 (see Table 3.2 of (Fugro, 2021)), and validation studies such as (TNO, 2021) show that for this type of LiDAR the accuracy of the measurement is not significantly sensitive to the value of the threshold. A thorough and quantitative overview of availability statistics for these instruments are provided in the references stated in Table 1. For comparisons with model data, the data have been hourly averaged and only time periods with at least 5 valid 10-minute timestamps data have been used.

1.3 Derivation of a 10m wind time series from measurements

As explained later in Sect. 3.2, when u_{*0}, L, and α_{Ch} are known, wind speed at any elevation in the surface layer can be computed (an example is given for the 26.1 m cup anemometers at IJM). Therefore, deriving a 10 m wind from measurement data is not always necessary.

However, for practical reasons this is needs to be done (CFSR and CFSv2 winds are available at 10 m, or, traditionally for spectral wave modelling). In the present article, two methods have been considered for every 10-minute timestamp: 1) interpolating using a power law the measurements between the 4 m sonic anemometers and the lowest LiDAR measurement elevation, and 2) fitting a power- or log law to the LiDAR measurements up to- and including 80 m, and then extrapolating down to 10 m. Both methods add some uncertainty to the derived 10 m value: for 1), the uncertainty mainly lies in the uncertainty of the 4m sonic anemometers; for 2), and in particular for stable conditions, the wind profile may not be well fitted by a power law. To alleviate these uncertainties, the present study focuses on wind speeds larger than 15 and 20 m/s (where stable conditions are very rare) and in Sect. 2.3 the comparison is made for unstable- and neutral conditions only by limiting the range of air-sea temperature difference to $\Delta\theta = T_{4\text{m}} - SST < [-2; 0.5]\,°C$ (North Sea) and $\Delta\theta = T_{4\text{m}} - SST < 0.5°C$ (Atlantic Bight). For all these comparisons, the mean wind speed measurement profile is provided to check the validity of the extrapolation method. Furthermore, the uncertainty of the extrapolation method has been verified using proprietary Fugro FLS measurements located in Northern Scotland where 12 m LiDAR measurements are available (the exact location is confidential): see Figure 3 which shows that the errors are the smallest when considering method 1). This method has thereby been chosen in Sect. 2.3, but it has been checked that the conclusions of the analysis are not sensitive to the choice of the method (i.e. that the ERA5 10 m wind speeds are smaller than measured values, also when considering measurement uncertainty).
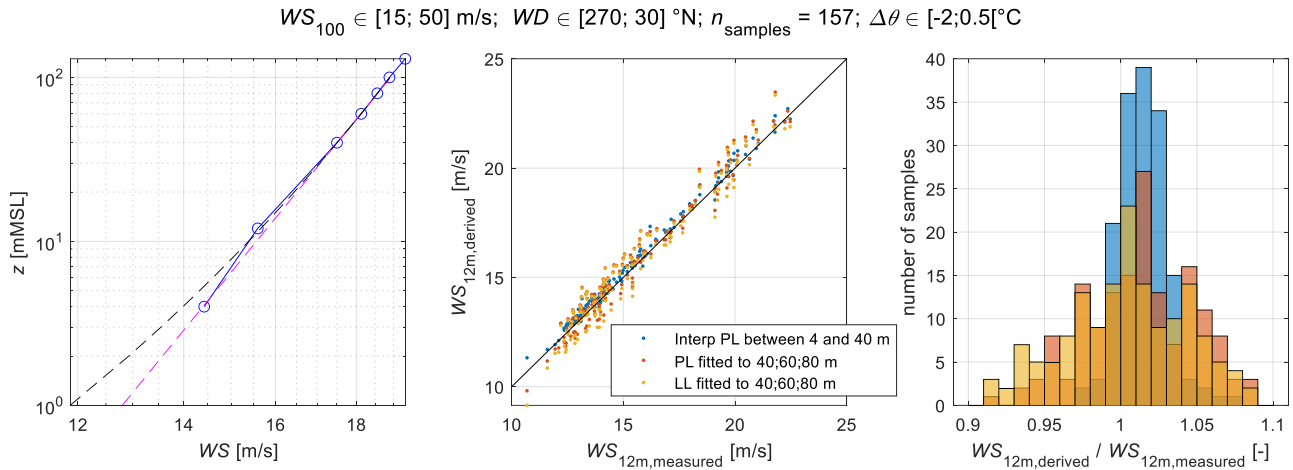
Figure 3: The middle- and right-hand side panels figure show comparisons of 12 m hourly wind speed measurements from a Fugro FLS (undisclosed location) with 12 m time series derived using the three methods discussed in the text and stated in the legend. The left-hand side panel shows the corresponding mean wind speed profile, where the blue markers are FLS measurements, the black line is the fitted log law and the magenta line the fitted power law.

1.3 Model data

For this study, CFSR (Saha et al., 2010) and CFSv2 (Saha et al., 2014) data have been downloaded using DHI's MetOcean On Demand (MOOD) web interface[3]. Data from ERA5 (Hersbach et al., 2020) have been downloaded from MOoD as well for the locations M6, Lot 1, Lot 2, E05 and E06. For the locations TNWA, IJM and 62001 the ERA5 data was also fetched from the Copernicus Data Store (CDS), and for these locations it was verified that both sources are identical.

2 Comparisons of ERA5 and CFSR / CFSv2 with measurements

In the literature, multiple comparisons between in-situ measurements and IFS model wind speed close the surface have concluded that for strong wind conditions the IFS model wind speeds are smaller than measured values and smaller than other reanalysis datasets (global, or regional), see for instance (Fery et al., 2018) for ERA Interim and (Bentamy et al., 2021), (Alday et al 2021), (Solbreke et al., 2021), (Spangehl et al., 2023), (Meyer et al., 2023) for ERA5.

2.1 Comparisons between ERA5 and CFSv2

Examples of differences with ERA5 (IFS) and CFSv2 (GFS) model results are provided below for two locations: the M6 buoy off the west coast of Ireland, and the TNW FLS; see Figure 4. Similar trends are visible across several locations in the northwest European shelf, see the supplementary material. Figure 5 shows that at the 62001 buoy location and when separating the dataset

---

[3] See https://www.metocean-on-demand.com/, where it is stated that "*The data is extracted as discrete (non-interpolated) values of the model grid cell.*"

155 between short- and long fetches, the ERA5 model results show larger differences for short fetches; as discussed in Sect. 3 this is the sign that the difference between the models is driven by the dependency of the ERA5 drag formulation to the sea state. This effect of the same magnitude at all locations when considering the CFSR data (1979-01-01 to 2011-04-01) which have a coarser resolution than ERA5, see the supplementary material provided with this paper.
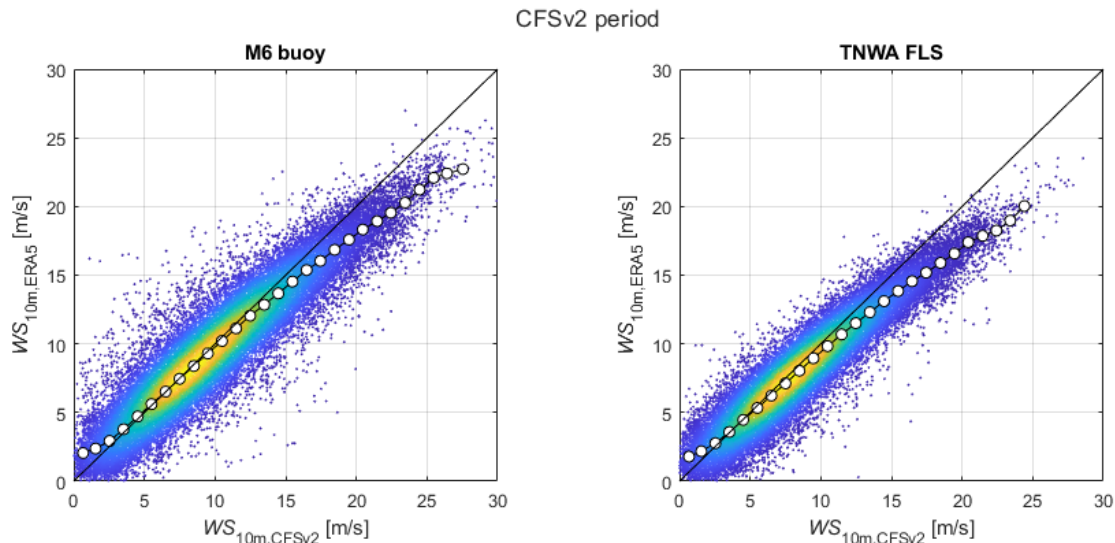
Figure 4: For two locations (see Figure 2), comparison of the ERA5 and CFSv2 10m wind speeds. For wind speeds above approximately 10 m/s, the ERA5 values are smaller than the CFSv2 values; this effect is stronger at TNWA than at M6. Also, this effect of the same magnitude when considering the CFSR data (1979-01-01 to 2011-04-01), which have a coarser resolution than ERA5.
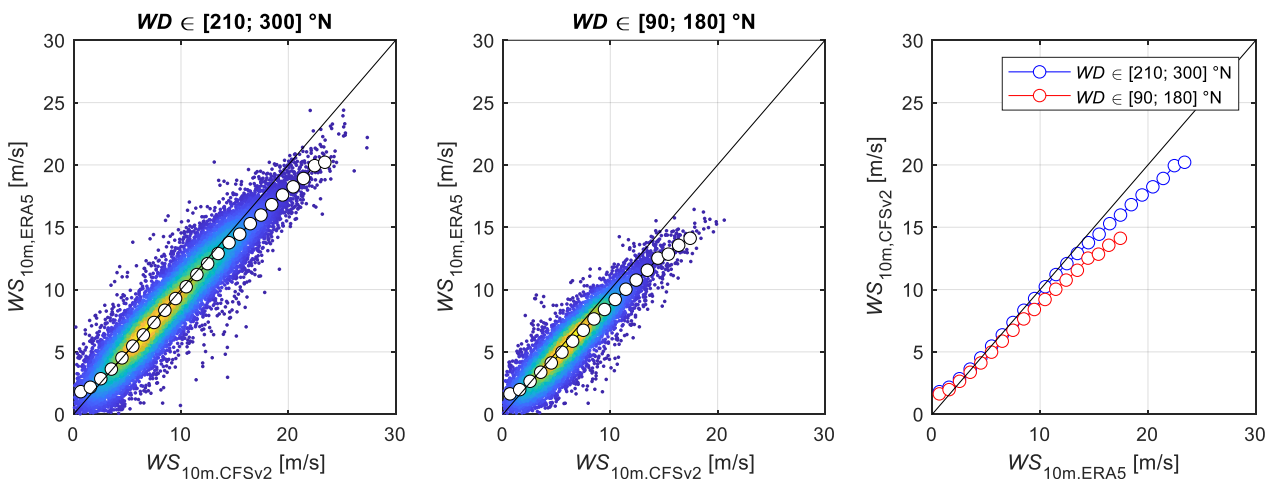
Figure 5: As for Figure 4, this figure shows a comparison of ERA5 and CFSv2 10m wind speeds, this time at the 62001 buoy and for two wind directional bins corresponding to very long fetch and short fetch. The difference between the two model results is larger for short fetches.

2.2 Comparisons between ERA5 and measurements

Using the method explained in Sect. 1.3, 10 m wind speed time series have been derived from FLS measurements. These
170 values compared with ERA5 and CFSv2 model data for 5 measurement locations in Figure 6 (Lot 1) and in Appendix A in
Fig. A3 to A6. For all locations, the ERA5 values are smaller than the measured values, and smaller than the CFSv2 values.
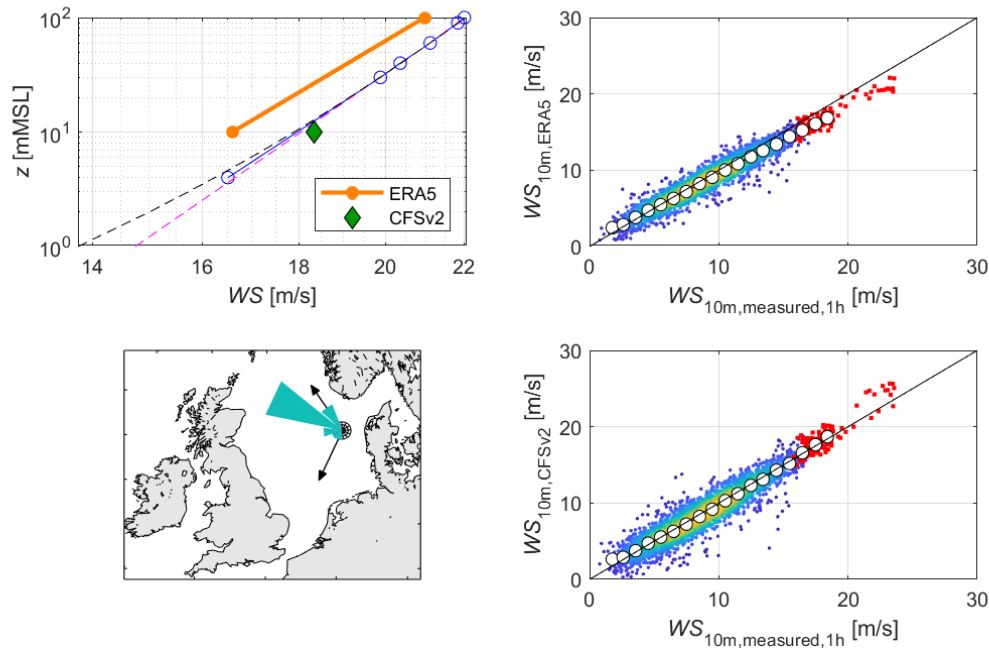
Figure 6: For one FLS location in the Danish North Sea, comparison between modelled and measured hourly mean wind speeds. A
175 **subset of large wind speeds (selected using the FLS measurements at 100m), are highlighted in red. The plot to the top-left shows**
mean wind speed profiles for this subset, where the blue line represents measurements. The dashed black line is a power law fit to
the measurement data below 80m, the magenta line represents a log law. The 10m measured data on the x-axis of the scatter plots
has been interpolated between the 4m sonic anemometer and the lowest LiDAR elevation; it can be checked on the top left that this
is a valid approach which introduce an uncertainty smaller than the difference between the two models. A wind rose corresponding
180 **to the subset of large wind speeds (in red on the scatter plots) is shown on the map.**

3 Addressing and correcting the ERA5 drag formulation.

In Sect. 3.1, using ERA5 data downloaded from the CDS, we check that ERA5 wind speeds can be derived from friction
velocity, Charnock parameter and the Obukhov length; then we analyze the behavior of the ERA5 drag formulation for
different sea state conditions and conclude that the ERA5 bias likely comes from the asymptotic behavior of Eq. (3) for large
185 values of τ_w/τ. Then, in Sect. 3.2 we propose a simple correction which consists of capping, or keeping constant, the values
of the Charnock parameter.

3.1 Drag formulation in ERA5

As explained in Sect. 1, friction velocity, roughness length and mean wind speed are interlinked via Eq. (1) and (2). On one
hand, the ERA5 analysis 10 m wind speed time series is readily available (via its two horizontal components) on the CDS. On
190   the other hand, friction velocity u_{*0} and roughness length z_0 are only provided as forecast values. Please note that this forecast
roughness length time series is faulty and should not be used[4]; instead, the best way to estimate z_0 from CDS data is to use the
Charnock coefficient time series (available from the CDS) and u_{*0} as in Eq. (2). As a result, ERA5 10 m wind speeds time
series can be reconstructed solely using Eq. (1) with u_{*0}, α_{Ch} and L computed from CDS data[5]: as shown in Figure 7 this gives
satisfactory results. Furthermore, the formulations presented in (Gryning and al., 2007) can be used for deriving very realistic
195   100 m wind speeds, see Figure 7 as well (this is helpful to practitioners who may want to derive wind speeds are larger
elevations).
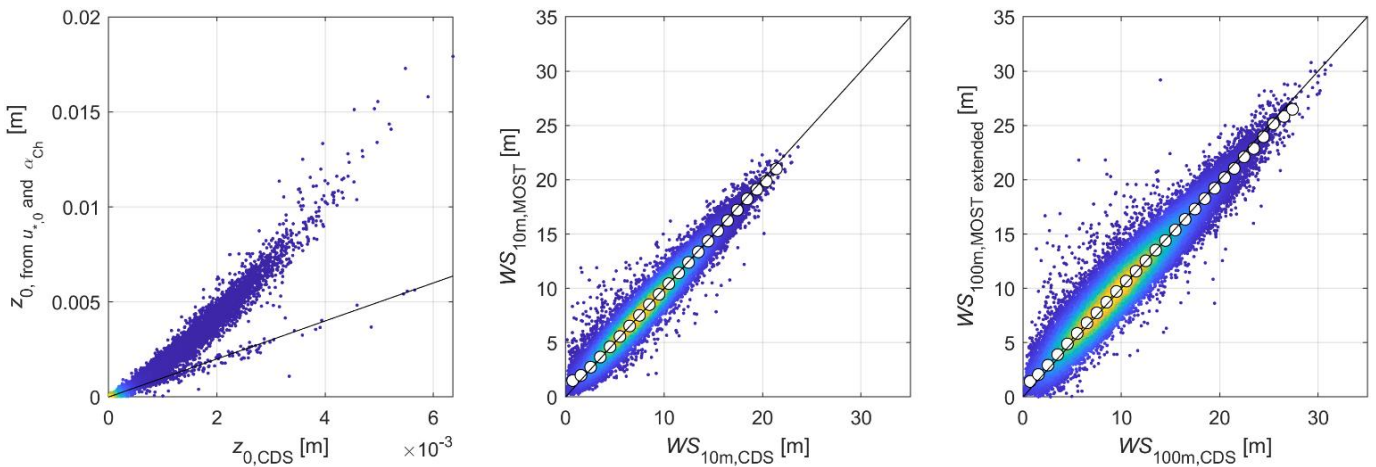
**Figure 7: For ERA5 at the TNWA location, the left-hand side of this figure shows comparisons between the roughness length values
200   from the CDS (faulty) and the ones computed using the friction velocity and the Charnock parameter time series. The plot in the
middle shows a comparison between the 10m wind speed from the CDS and the one derived using MOST with the friction velocity,
the roughness length derived from friction velocity and Charnock parameter, and the Obukhov length computed from CDS time
series. The plot to the right shows a comparison between the 100m wind speed time series from the CDS and the one derived from
the same parameters as for the middle plot, plus the surface layer extension model from (Gryning et al, 2007). Overall, this figure
205   shows that the wind speed values from the CDS at 10 and 100m can easily be reproduced using well known wind profile expressions.**

---

[4] Item 18 on https://confluence.ecmwf.int/display/CKB/ERA5%3A+data+documentation#ERA5:datadocumentation-Knownissues.
[5] For the present study, we have used u_{*0}, and the sensible heat flux, the air- and dew point temperature at 2 m as well as the
surface pressure.

3.2 Bias explanation and correction

From the above discussion, the results of the ERA5 drag formulation can be analysed further, with regards to Eq. (3) and the sea state dependency of the Charnock parameter. For increasing values of τ_w/τ, the resulting value of z_0 has been computed

210   for a wide range of 10 m wind speeds using Eq. (1) (2) iteratively, and the results are shown against ERA5 time series at TNWA and the 62001 buoy in Figure 8. For strong wind speeds the z_0 values are relatively larger for the former than for the later, and for large values of τ_w/τ, small changes of this ratio lead to very large changes in z_0: for instance, at 15 m/s, a change from 0.99 to 0.995 in τ_w/τ lead to 60% increase in z_0. Since, as shown in Figure 9, the ERA5 and CFSR/CFSv2-derived friction velocity values are similar, this increase in roughness length leads to a decrease in mean wind speed.
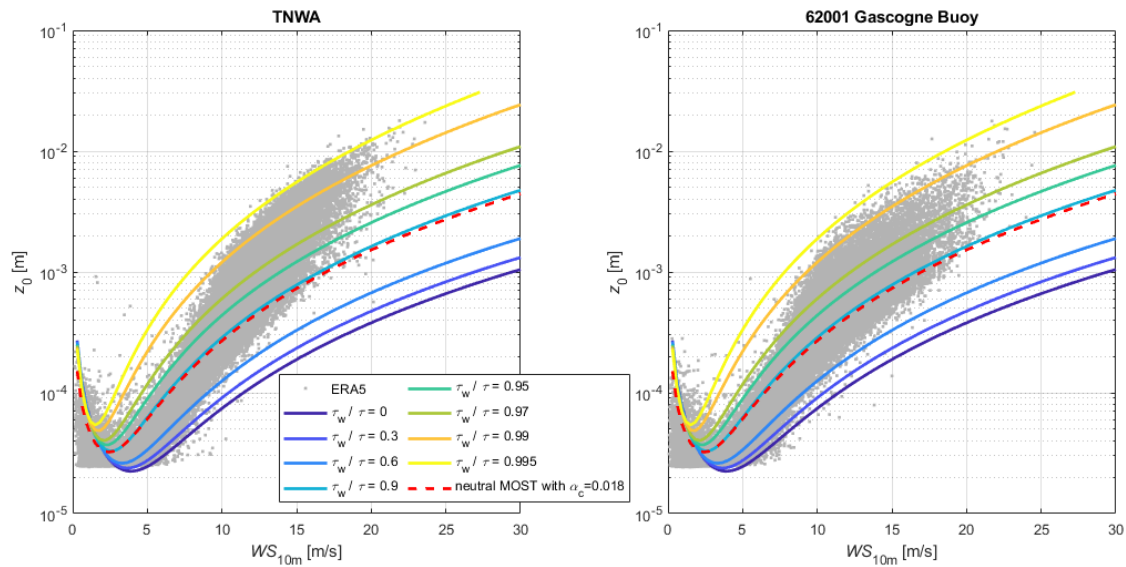
215

Figure 8: For two locations, this figure shows a scatter plot of ERA5 roughness lengths values against 10m wind speed. Using an iterative process, Eq. (1), (2) and (3) have been solved for different values of ratios between wave- and wind stress, and for a constant Charnock parameter value of 0.018; the results are shown on the figures.

In IFS, as τ_w/τ increases, the Charnock coefficient increases; Figure 10 shows that this is particularly the case for short fetch

220   conditions in relatively shallow waters like the North Sea. For such conditions and for a given value of significant wave height, the peak period of the spectra is typically smaller than for fully developed, long fetch conditions. The bias in IFS may then be related to the growth rate parameterisation described in Sect. 2.2 of (ECWMF, 2016b). This should be investigated in future works, for instance in ERA6 and ERA7 pre-production validation studies; see Sect. 4.
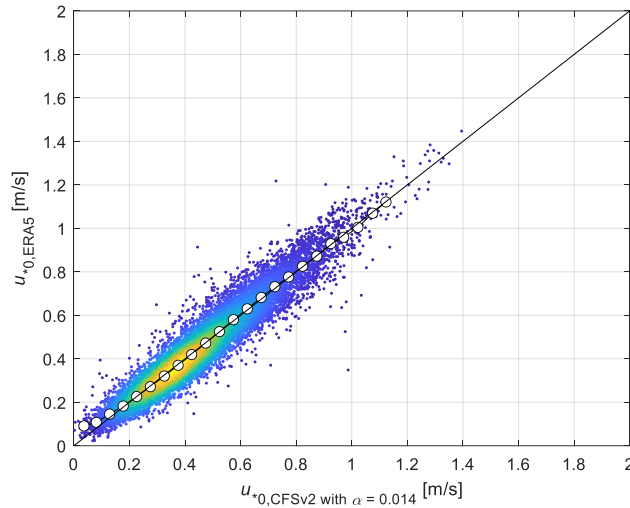
225

Figure 9: For the TNWA FLS location and for neutral conditions, this figure shows a comparison between friction velocities values from the ERA5, and the ones derived iteratively using Eq. (1) and (2) and the 10 m CFSv2 wind speed time series (with a constant Charnock coefficient of 0.014, see (Renfrew et al., 2002)
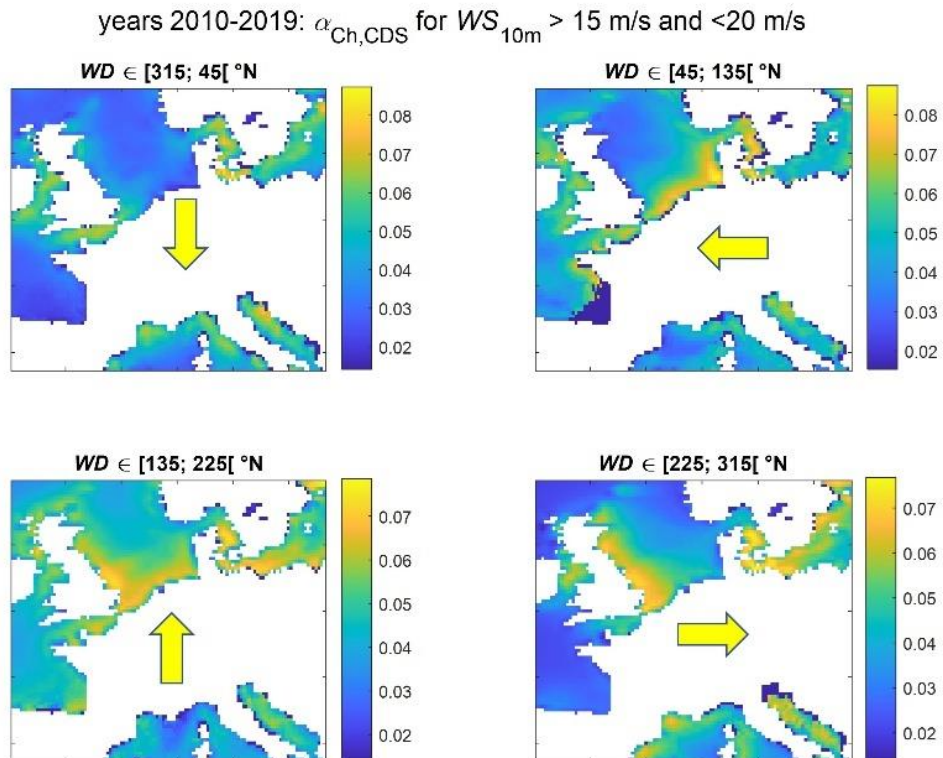
230   **Figure 10: This figure shows mean values of ERA5 Charnock coefficient for strong wind speed conditions, and four different wind directional bins.**

3.3 Bias correction

From the above, we conclude that CFSv2 and ERA5 can come to a closer agreement when changing the value of the ERA5 Charnock parameter. This is demonstrated in Figure 11, where ERA5 α_{Ch} values are set to 0.018, and 10 m ERA5 wind speeds
235   are derived as explained in the previous section.
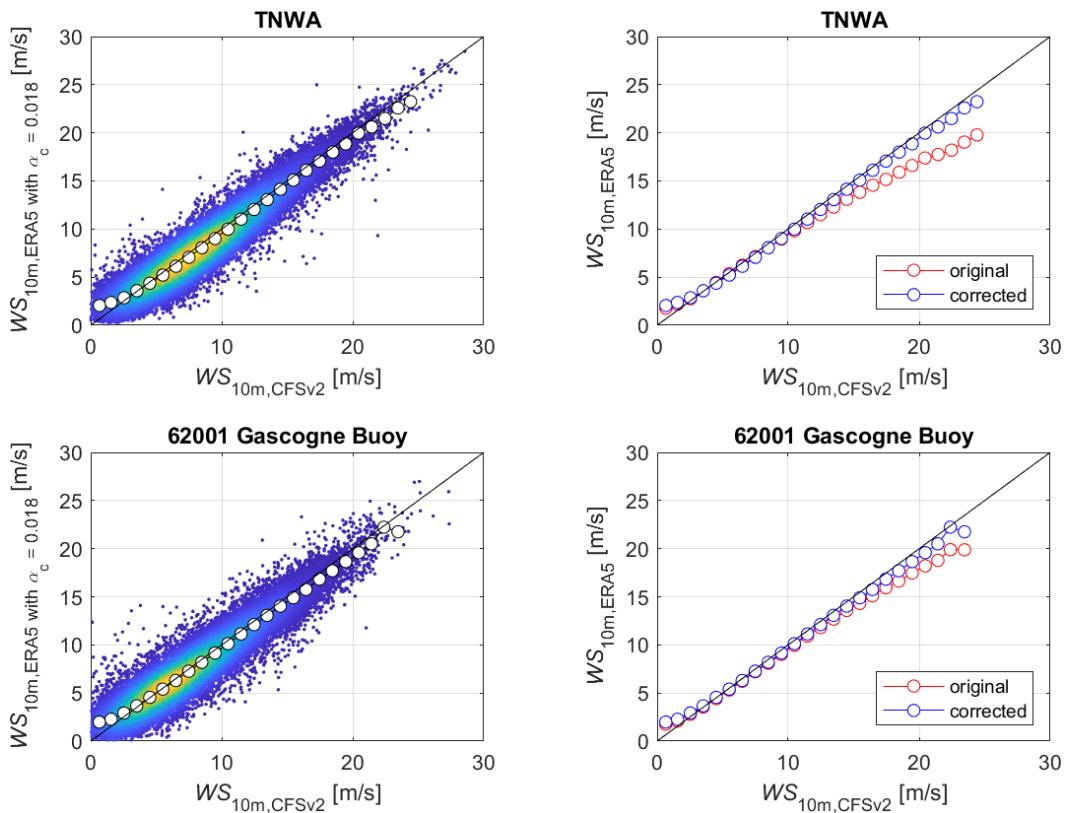
Figure 11: This figure shows comparison of ERA5 10m wind speeds computed, as explained the text, using the CDS friction velocity and Charnock parameter capped at 0.018 and the CFSv2 time series. This method reduced greatly the difference at large wind
240   **speeds.**

Furthermore, this methods allows a direct comparison of ERA5 values with measurements, without having to extrapolate the measurement elevation: see the example of the 26.1m anemometer time series at the IJmuiden mast in Figure 12, where four time series are compared: original ERA5 (top-left), ERA5 with constant $\alpha_{Ch} = 0.018$ (top-right), ERA5 with $\max(\alpha_{Ch}) = 0.018$ (bottom-left) and the method employed in the Global Atlas of Siting Parameters Ocean and Coast (GASPOC) project
245   (DHI, 2023) for their "*modified*" ERA5 wind speed time series (bottom-right). This last method uses ERA5 wind speed and atmospheric stability information only (not α_{Ch} nor u_{*0}), and it leads therefore to larger wind speeds in strong wind conditions.
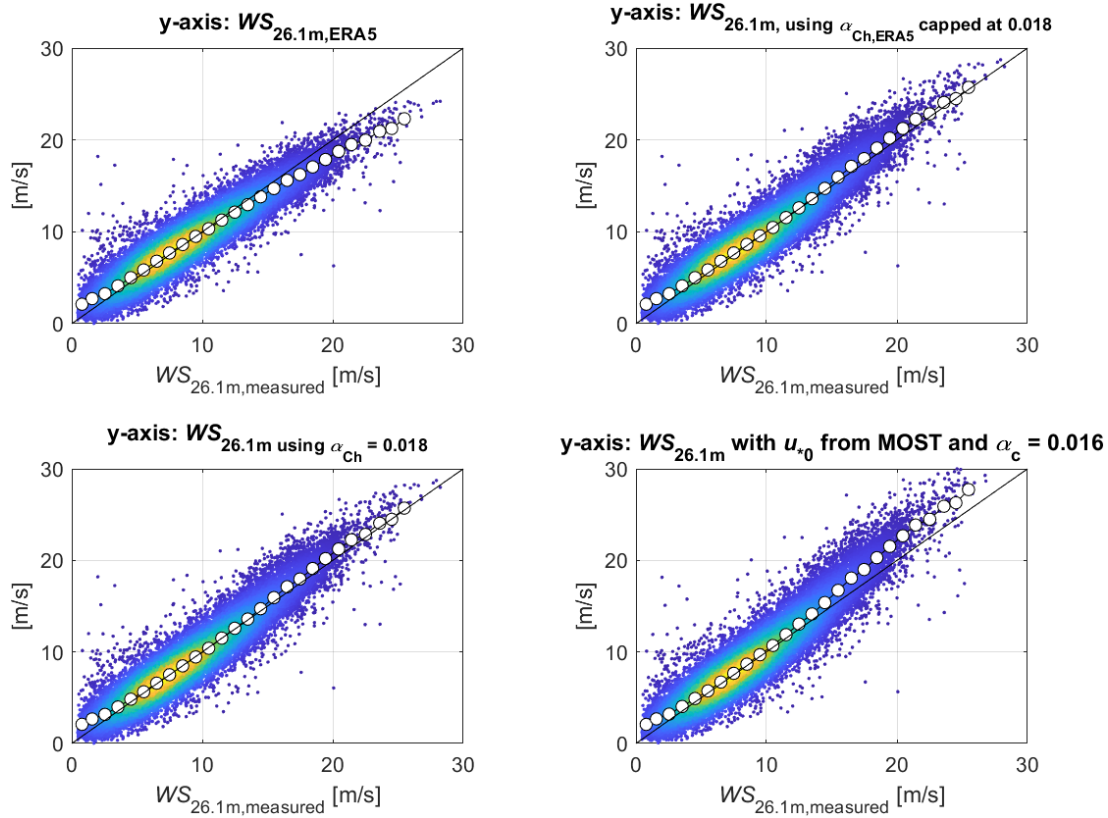
Figure 12: This figure shows comparison of ERA5 26.1m wind speeds and measurements at 26.1 m from the Ijmuiden mast. The model data are computed as explained the text and summarized in the title of the subplots.

4 Conclusion and suggestions for future work

The characterisation of the interactions between wind, sea state and currents remains an active field of research. Flux measurements experiments have been carried out at a few locations only, and the theoretical basis for understanding these interactions is still developing (Ayet and Chapron, 2022), (Janssen and Bidlot, 2023).

Modellers have adapted these models to one- or two-way coupled atmosphere-ocean modelling systems, and comparisons are regularly performed, see for instance (Edson et al, 2013) and (Bouin et al,, 2024). These comparisons are often carried out for locations that are not representative of Offshore Wind locations. For instance, the ECWMF drag formulation in (Edson et al., 2013) is representative of the "*globally averaged wave age–dependent roughness at a given wind speed*". As oceans cover 70% of the globe, these model grid cells are in their vast majority deep water, very far offshore locations where the fetch- and bathymetry dependent bias discussed in Sect. 3 is less visible. Or, in (Bouin et al,, 2024) and (Janssen and Bidlot, 2023), the focus is set on very large wind speeds during Tropical Cyclones (TC); this is a valuable for the forecasting community but offshore wind applications require the entire range of wind speeds to be modelled accurately.

Some may argue that when focusing on modelling sea state hydrodynamic conditions, adjustments to the wind forcing are equally important as the other wave spectra sources and sinks of energy (bottom friction, wave-wave interactions, etc). This is

265 true, but the end-users and in particular offshore wind practitioners, require both wind and waves/hydrodynamics to be correct. As the next generation of high resolution (towards km-scale) reanalysis datasets are being prepared for production (ERA6/7, MERRA-3) planning for sector- or class of user-specific validations becomes necessary, for instance and with increasing complexity:

➤ Validation runs against mast, LiDAR and FLS measurements during a great number of storm events (this is commonly
270   done for commercial projects). Adding such datasets alongside legacy measurements such as met buoys, would prove very valuable and persuasive towards wind energy practitioners. On the other hand, oceanographers who are relying in legacy measurement would find an alternative, higher quality datasets to work with.

➤ Refined grid meshes in coastal areas where offshore wind projects are being developed and adapting model data delivery to the needs of offshore wind practitioners.

275 ➤ Including LiDAR measurements in air-sea interaction measurement campaigns (as in the WFIP3 project[6]).

➤ Continuing working towards unifying oceanographic and ABL meteorology frameworks, from a wind energy perspective as discussed in (Shaw et al. 2022).

---

[6] See https://www.psl.noaa.gov/renewable_energy/wfip3/.

Appendix A
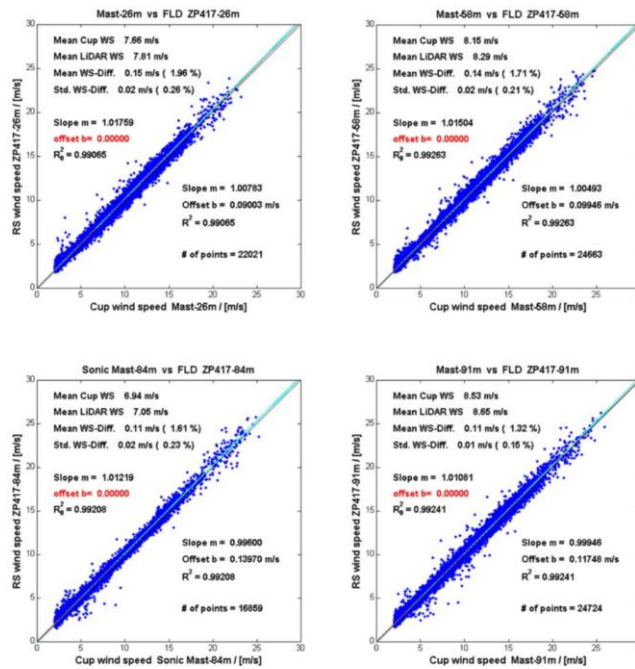
280

Figure A1: Example of FLS LiDAR validation, from (GLGH, 2015)
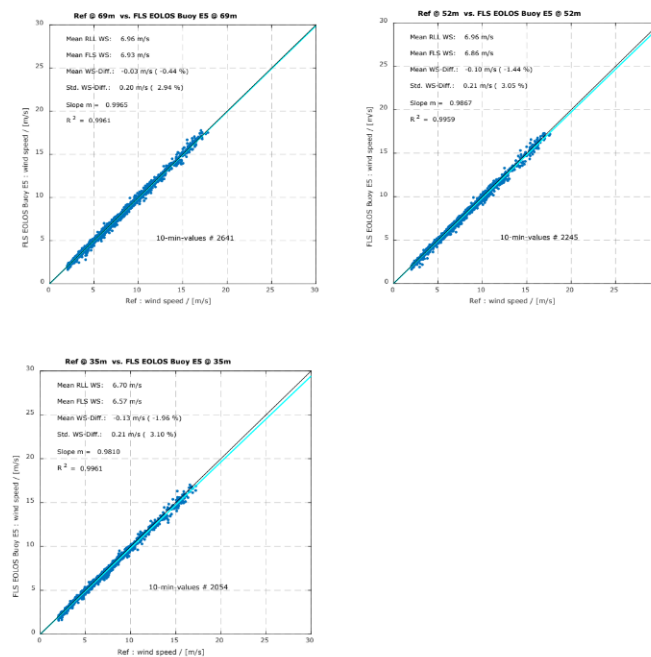
Figure A2: Example of FLS validation, from (DNV GL, 2019)
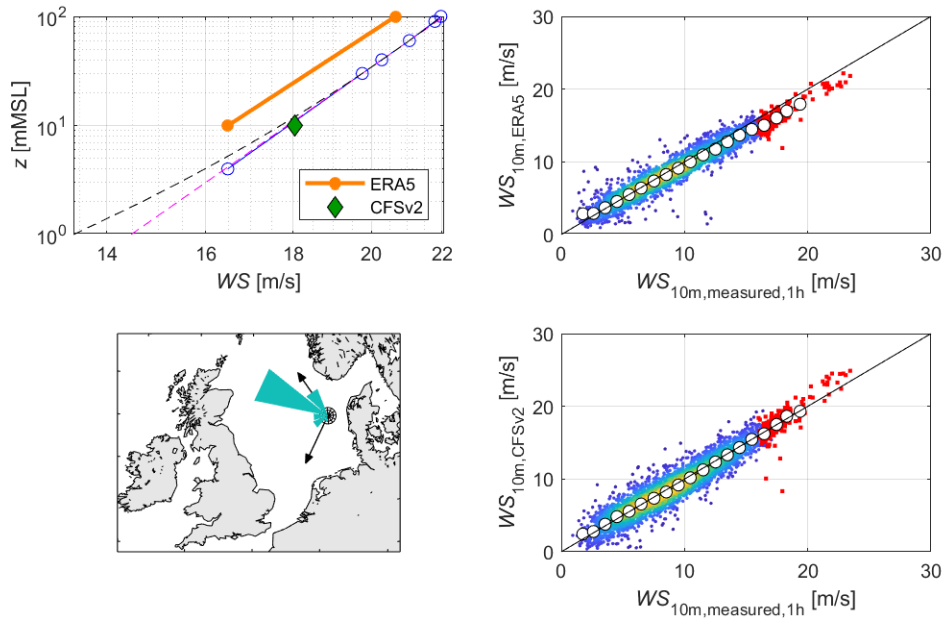
285

Figure A3: Same as Figure 6, but for the Lot2 FLS location in the Danish North Sea.
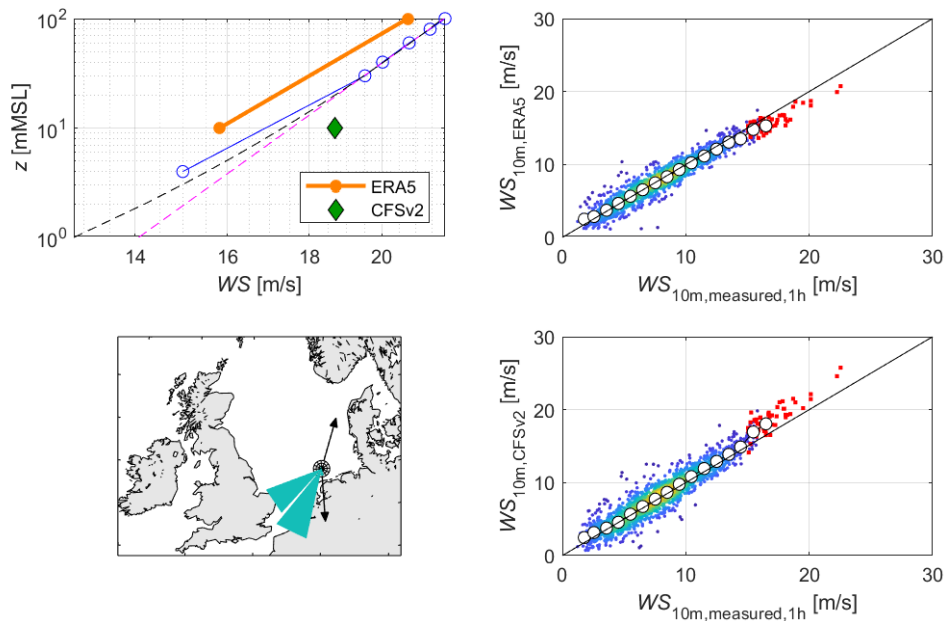
Figure A4: Same as Figure 6, but for the TNWA location in the Danish North Sea.

290
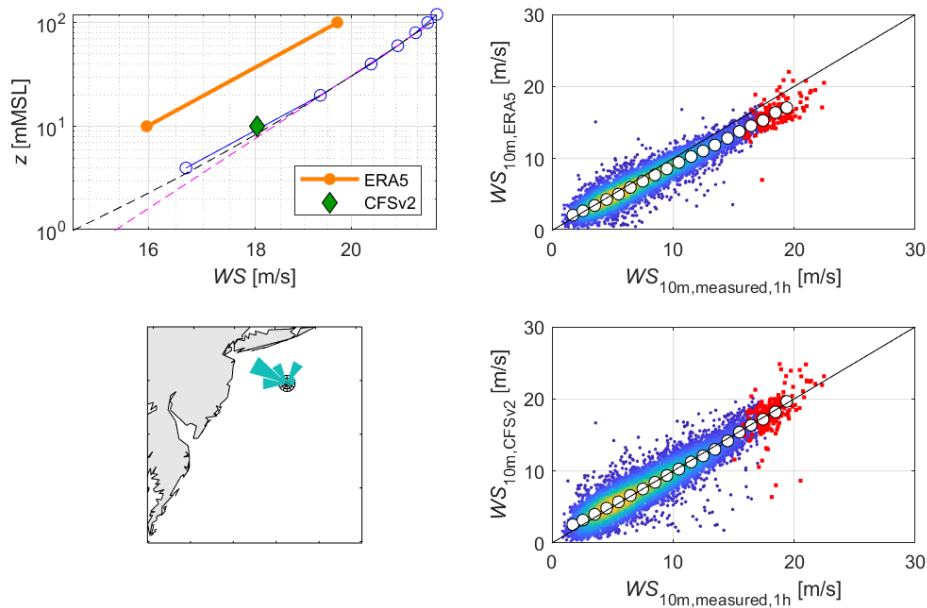
Figure A5: Same as Figure 6, but for the E05 FLS location in the New York Bight.
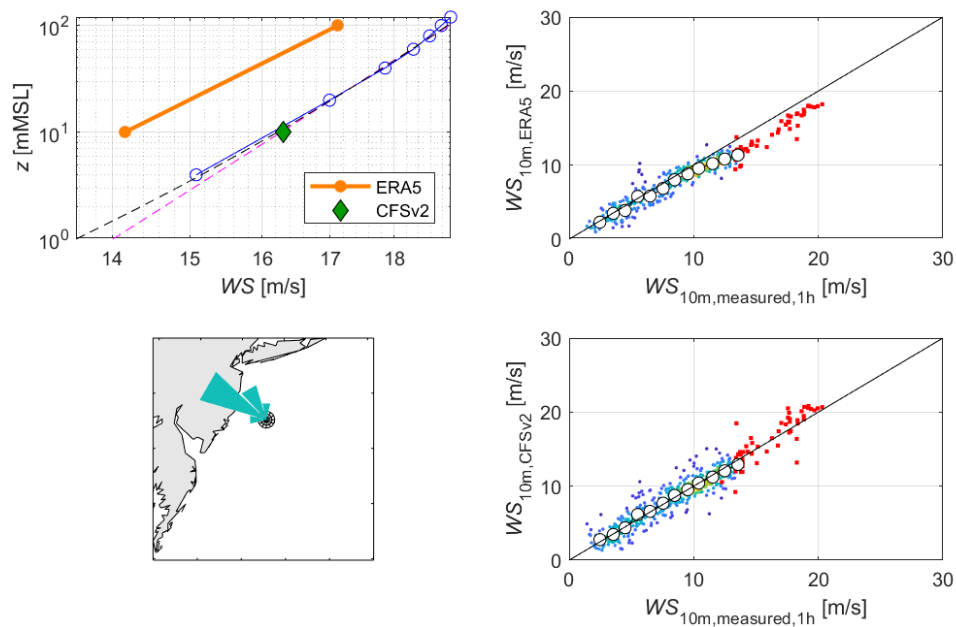
295 **Figure A6: Same as Figure 6, but for the E06 FLS location in the New York Bight.**

Code and data availability

The analysis was carried out in MATLAB. The code is not available, as some of the functions are proprietary to C2Wind ApS. The data are publicly available, see the references in the article.

Author contribution

300 RG conceptualised the article and carried out the analysis. JG reviewed the manuscript.

Competing interests

The authors declare that they have no conflict of interest.

Acknowledgements

The authors would like thank Jean Bidlot for his patience and his interest in Offshore Wind applications.

305 **Supplementary material**

Publicly available LiDAR and FLS validation reports, as well as comparisons of ERA5 and CFSR/CFSv2 10 m wind speeds as several locations are provided in the following Zenodo repository.

Gandoin, R. Supplementary material to the Wind Energy Science article "Underestimation of strong wind speeds offshore in
310 ERA5: evidence, discussion, and correction". Zenodo. https://doi.org/10.5281/zenodo.10800232, 2024.

References

Alday M., Accensi M., Ardhuin F. and Dodet G. A global wave parameter database for geophysical applications. Part 3: Improved forcing and spectral resolution. Ocean Modelling. doi:/10.1016/j.ocemod.2021.101848, 2021.

315 Araújo da Silva, M.P., Rocadenbosch, F., Farré-Guarné, J., Salcedo-Bosch, A., González-Marco, D., Peña, A. Assessing Obukhov Length and Friction Velocity from Floating Lidar Observations: A Data Screening and Sensitivity Computation Approach. Remote Sens. 14, 1394, doi:10.3390/rs14061394, 2022.

Ayet, A., Chapron, B., The dynamical coupling of wind-waves and atmospheric turbulence: a review of theoretical and
320 phenomenological models. Bound.-Layer Meteorol., 2022

Bentamy, A., Grodsky, S.A., Cambon, G., Tandeo, P., Capet, X., Roy, C., Herbette, S., Grouazel, A. Twenty-Seven Years of Scatterometer Surface Wind Analysis over Eastern Boundary Upwelling Systems, Remote Sens., 13, 940, doi:10.3390/rs13050940, 2021.

325

Bidlot, J-R et al. Inter-comparison of operational wave forecasting systems. 10th Wave Worksho., November 11-16, 2007.
North Shore, Oahu, Hawaii, USA,
http://www.waveworkshop.org/10thWaves/Papers/paper_10th_workshop_Bidlot_at_al.pdf, 2017.

330   Carbon Trust. Carbon Trust Offshore Wind Accelerator Roadmap for Commercial Acceptance of Floating LiDAR
Technology. Version 2.0, https://www.carbontrust.com/our-work-and-impact/guides-reports-and-tools/roadmap-for-
commercial-acceptance-of-floating-lidar, 2018-10.

DHI. EUDP Global Atlas of Siting Parameters Offshore. ERA5 Wind: Validation and Comparison. Report, Accessed via
335   https://www.metocean-on-demand.com/, 2023.

DNV GL: Assessment of EOLOS FLS-200 E05 Floating Lidar Pre-Deployment Validation at the Narec NOAH Offshore
Met Tower, UK. Report No.: 02, Rev. A. Document No.: 10124962-R-2-A,
https://oswbuoysny.resourcepanorama.dnv.com/download/f67d14ad-07ab-4652-16d2-08d71f257da1, 2019.

340
ECMWF. IFS Documentation – Cy41r2. Operational implementation 8 March 2016. Part IV: Physical Processes,
https://www.ecmwf.int/en/elibrary/79697-ifs-documentation-cy41r2-part-iv-physical-processes, 2016a.

ECMWF. IFS Documentation – Cy41r2. Operational implementation 8 March 2016. Part VII: ECMWF Wave Model,
345   https://www.ecmwf.int/en/elibrary/79700-ifs-documentation-cy41r2-part-vii-ecmwf-wave-model, 2016b.

Edson, J. B., Jampana, V., Weller, R. A., Bigorre, S. P., Plueddemann, A. J., Fairall, C. W., Miller, S. D., Mahrt, L., Vickers,
D., & Hersbach, H. On the Exchange of Momentum over the Open Ocean. Journal of Physical Oceanography, 43(8), 1589-
1610. doi:/10.1175/JPO-D-12-0173.1, 2013.

350
ENTSO-E. TYNDP 2024. Offshore Network Development Plans European offshore network transmission infrastructure
needs. Pan-European summary, 2024.

EOLOS. NYSERDA Measurement Plan. Code: EOL-NYS01. Revision 02,
355   https://oswbuoysny.resourcepanorama.dnv.com/download/f67d14ad-07ab-4652-16d2-08d71f257da, 2020

Fery, N., Tinz, B., Ganske, A., Gates, L. Reproduction of 10m-wind and sea level pressure fields during extreme storms with
regional and global atmospheric reanalyses in the North Sea and the Baltic. 2nd Baltic Earth Conference,
doi:10.13140/RG.2.2.24884.35200, 2018.

360
Fugro, Supply of Meteorological and Oceanographic data at Hollandse Kust (west), 24-month summary campaign report:
5 February 2019 - 11 February 2021, Fugro Document No: C75432_24M_F,
https://offshorewind.rvo.nl/file/download/498241e9-bdb1-45ce-8343-
303727e620a7/1639050959hkw_20211125_mc_fugro_24m%20report_f.pdf, 2021.

365
Fugro. Supply of Meteorological and Oceanographic data at Ten noorden van de Waddeneilanden 24-month summary
campaign report: 19 June 2019 - 20 June 2021 Fugro Document No: C75433_24M_F,
https://offshorewind.rvo.nl/file/download/3b2f655f-af72-4bf5-9754-a7d2d2e6dc6c/tnw_20220118_mc_fugro_report-f.pdf,
2022.

370
Fugro. SWLB measurements at Energy Islands. Project Measurement Plan, All Lots.
C75486_Project_Measurement_Plan_All_Lots 09. Final. Accessed from ENS's FTP https://ens.dk/en/our-
responsibilities/offshore-wind-power/preliminary-site-investigations-energy-islands-0, 2023.

375   GLGH: Assessment of the Fugro/Oceanor Seawatch Floating LiDAR Verification at RWE IJmuiden met mast. Technical Note No.: GLGH-4257 13 10378-R-0003, Rev. B., https://offshorewind.rvo.nl/file/download/ae688c2d-721f-416c-8902-51f0c0f5bf63/1502435907hkz_20150130_dnvgl_ijmuiden%20trial%20campaign%20validation-f.pdf, 2015.

Gryning, S-E., Batcharova, E., Brümmer, B., Jørgensen and H., Larsen S. On the extension of the wind profile over
380   homogeneous terrain beyond the surface boundary layer. Boundary-Layer Meteorology, 2007.

Hersbach H., et al. The ERA5 global reanalysis. Quaterly Journal of the Royal Meteorological Society, 2020.

Janssen, P. A. E. M., & Bidlot, J. Wind–Wave Interaction for Strong Winds. Journal of Physical Oceanography, 53(3), 779-
385   804. doi:10.1175/JPO-D-21-0293.1, 2023.

Kelberlau, F. and Mann, J.: Quantification of motion-induced measurement error on floating lidar systems, Atmos. Meas. Tech., 15, 5323–5341, doi:10.5194/amt-15-5323-2022, 2022.

390   Kelberlau, F.: Floating Lidar Systems. Measurement accuracy under strong wind conditions. WRM Discussion group meeting, 2022-03-30. Link: https://oceanalysis-my.sharepoint.com/:f:/p/gus_jeans/Ep9M6eSQXPZLl9-fNpZ_7mMBDpRKZ8KEu_yXoMeN5e5ZdQ, 2022.

Knoop, S., Bosveld, F. C., de Haij, M. J., and Apituley, A.: A 2-year intercomparison of continuous-wave focusing wind
395   lidar and tall mast wind measurements at Cabauw, Atmos. Meas. Tech., 14, 2219–2235, doi:/10.5194/amt-14-2219-2021, 2021.

Meyer, E. M. I. and Gaslikova, L.: Investigation of historical severe storms and storm tides in the German Bight with century reanalysis data, EGUsphere [preprint], doi:/10.5194/egusphere-2023-2068, 2023.
400
Ortiz-Suslow, D. G., Kalogiros, J., Yamaguchi, R., and Wang, Q. An evaluation of the constant flux layer in the atmospheric flow above the wavy air-sea interface. Journal of Geophysical Research: Atmospheres, 126, e2020JD032834. doi:/10.1029/2020JD032834, 2021.

405   Peña, A., Gryning, S-E. and Hasager C. Measurements and Modelling of the Wind Speed Profile in the Marine Atmospheric Boundary Layer. Boundary-Layer Meteorology, 2008

Quaeghebeur, E. and Zaaijer, M. B.: How to improve the state of the art in metocean measurement datasets, Wind Energ. Sci., 5, 285–308, doi:/10.5194/wes-5-285-2020, 2020.
410   Renfrew, I. A., Moore, G. W. K., Guest, P. S., and Bumke, K. A Comparison of Surface Layer and Surface Turbulent Flux Observations over the Labrador Sea with ECMWF Analyses and NCEP Reanalyses. Journal of Physical Oceanography, 32(2), 383-400. doi:/10.1175/1520-0485(2002)032<0383:ACOSLA>2.0.CO;2, 2002.

Ramon, J., Lledó, L., Torralba, V., Soret, A., Doblas-Reyes, FJ., What global reanalysis best represents near-surface winds?
415   Q J R Meteorol Soc, 145: 3236–3251, doi/10.1002/qj.3616, 2019.

Ruju, A., Filipot, J-F., Bentamy A., Leckler F. Spectral wave modelling of the extreme 2013/2014 winter storms in the North-East Atlantic. Ocean Engineering. doi:/10.1016/j.oceaneng.2020.108012, 2020.

420   Saha, S., and Coauthors: The NCEP Climate Forecast System Reanalysis. Bull. Amer. Meteor. Soc., 91, 1015–1058, doi:10.1175/2010BAMS3001.1, 2010.

Saha, S., and Coauthors: The NCEP Climate Forecast System Version 2. J. Climate, 27, 2185–2208, doi:/10.1175/JCLI-D-12-00823.1, 2014.

425

Shaw, W. J., Berg, L. K., Debnath, M., Deskos, G., Draxl, C., Ghate, V. P., Hasager, C. B., Kotamarthi, R., Mirocha, J. D., Muradyan, P., Pringle, W. J., Turner, D. D., and Wilczak, J. M.: Scientific challenges to characterizing the wind resource in the marine atmospheric boundary layer, Wind Energ. Sci., 7, 2307–2334, doi:/10.5194/wes-7-2307-2022, 2022.

430 Solbrekke, I. M., Sorteberg, A., and Haakenstad, H.: The 3 km Norwegian reanalysis (NORA3) – a validation of offshore wind resources in the North Sea and the Norwegian Sea, Wind Energ. Sci., 6, 1501–1519, doi:/10.5194/wes-6-1501-2021, 2021.

Spangehl, T., Borsche, M., Niermann, D., Kaspar, F., Schimanke, S., Brienen, S., Möller, T., and Brast, M.: Intercomparing 435 the quality of recent reanalyses for offshore wind farm planning in Germany's exclusive economic zone of the North Sea, Adv. Sci. Res., 20, 109–128, doi:/10.5194/asr-20-109-2023, 2023.

Stull R. An introduction to boundary layer meteorology, 1988.

440 TNO, Validation of the TNO ZX300 LiDAR system unit 308 at the TNO RSD Verification Facility Period: July 2019 to September 2019. TNO 2021 R10132, https://www.windopzee.net/wp-content/uploads/2021/03/mm6_zx308_2020.pdf, 2021.